We are IntechOpen, the world's leading publisher of Open Access books Built by scientists, for scientists

4,800
Open access books available

122,000
International authors and editors

135M
Downloads

Our authors are among the

154
Countries delivered to

TOP 1%
most cited scientists

12.2%
Contributors from top 500 universities

CLARIVATE ANALYTICS BOOK CITATION INDEX INDEXED

WEB OF SCIENCE™

Selection of our books indexed in the Book Citation Index in Web of Science™ Core Collection (BKCI)

Interested in publishing with us?
Contact book.department@intechopen.com

Numbers displayed above are based on latest data collected.
For more information visit www.intechopen.com

9

Coordinate Transformation Based Contour Following Control for Robotic Systems

Chieh-Li Chen and Chao-Chung Peng
Department of Aeronautics and Astronautics, National Cheng Kung University
No. 1 University Road, Tainan City 701,
Taiwan

1. Introduction

Robots are important for industrial automation. Similar to CNC machining, robotic systems can be applied to numerous applications such as material assembling, welding, painting, manufacturing and so on. For control of robot manipulators, a conventional way is to establish their mathematical models in the joint space and therefore precise positioning of end-effector relies on control performance in the joint space.
In terms of utilizations of industrial robots, it is well known that the position of end-effector is an important factor and significantly dominates the quality of final product. Based on given trajectories in work space (also known as Cartesian space), there are two main approaches for manipulator motion control, 1) one is to determine the desired joint space positions by solving the inverse kinematics, 2) the other is to consider the dynamic model in the work space directly (Feng & Palaniswami, 1993). In both approaches, tracking performance should be good enough in order to follow real time commands and achieve prescribed contours. In respect of the joint space approach, for instance, providing the tracking errors of each joint position can not be eliminated well, the end-effector can not track the desired profile precisely; to put it another way, once good tracking capability in any one of robot arms can not be guaranteed, the synchronization control task fails and thereby gives rise to unsatisfactory machining result. Consequently, it is worthy to investigate a better control strategy to guarantee the machining quality even in the presence tolerable tracking errors. To achieve this goal, we have to deviate the topic regarding control of robotic systems for a moment and address a certain core issues about contouring control systems.

1.1 Definition of contour error

First of all, a machining quality index called contour error is introduced. As shown in Fig. 1, the contouring error ε_p corresponding to point $P(t)$ is defined geometrically as the shortest distance from $P(t)$ to the desired contour D and can be written as $\varepsilon_p = \min_D \left\| P^* - P(t) \right\|$, where $P(t) \in S$ is the actual position of end-effector at time t and $P^* \in D$. Once the shortest

target P^* is found, (ideal) resultant control effort will force P(t) moving towards P^* firstly and then keep it attaching on the prescribed path. This control behavior involves two stages i.e., normal and tangential errors reduction. This concept is clear and has been widely used in contouring control designs (Koren, 1980; Chin & Lin, 1997; Ho et al., 1998; Yeh & Hsu, 1999; Chiu & Tomizuka, 2001, Shih et al., 2002; Wang & Zhang, 2004; Hsieh et al., 2006; Peng & Chen, 2007a; Peng & Chen, 2007b; Chen & Lin, 2008).

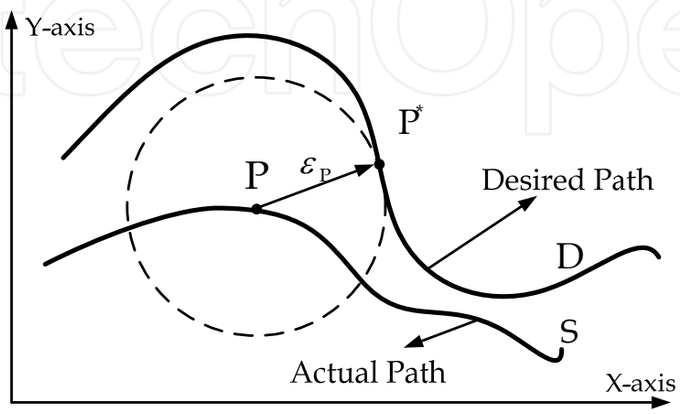

Fig. 1. Definition of contour error.

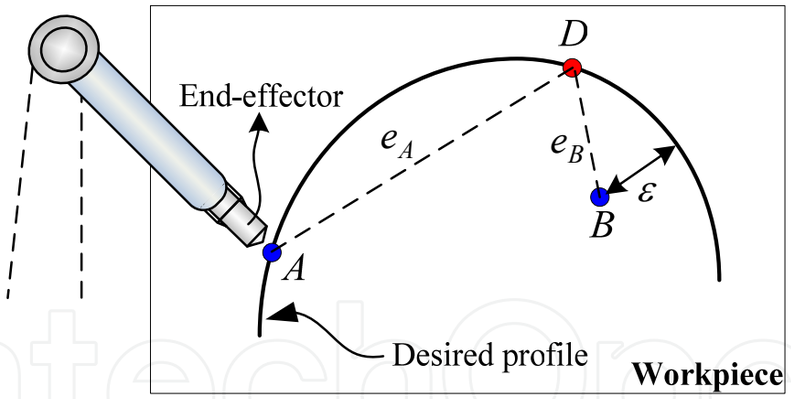

Fig. 2. Special issues appeared in contour following control systems.

1.2 Tracking and contouring control

Based on the definition of contour error, the following is to illustrate a main discrepancy between tracking control and contouring control. Consider Fig. 2, suppose that A is the location of the end-effector and D is the corresponding command position at a certain time instant. Providing the tracking error e_A exists significantly, a resultant tracking control force, where the orientation is towards from A to D, is going to be generated by controllers such that an undesirable working path away from the desired profile is induced. Moreover, Fig. 2 also reveals that a good tracking performance is just a sufficient, but not necessary, condition to reach good contouring performance. For example, the tracking error at point A

is apparently larger than the one at point *B*, but from contouring control point of view, contouring error is defined as the shortest distance from the end-effector to the desired path, so the position *A* is preferable in the contouring process rather than *B*. A couple of features and problems of contour control systems can be found in the tutorial study by Ramesh et al (2005).

1.3 Contouring control strategies

In terms of the literature on contouring control strategies, a well known cross-coupling control (CCC) structure (Koren, 1980) has been widely applied. Using this framework, contouring error attenuation can be carried out by designing various control strategies. For example, to raise machining speed, a modified CCC structure, where an additional pre-compensated controller is involved, called cross-coupled pre-compensation method (CCPM) (Chin & Lin, 1997) was proposed. However, these control components, namely tracking controller, contouring controller and feed-forward controller, are usually designed independently such that the coupling effects between them are not manifest. It is difficult to distinguish which one dominates the eventual contouring result. Thus, a systematic design procedure for CCC structure is highly desirable. To this end, transfer function methods for CCC structure are proposed (Yeh & Hsu, 1999; Shih et al., 2002; Zhong et al., 2002). These methods make the CCC design into a unit feedback control problem and offer a systematic analysis for stability and performance of a linear contouring system. However, superior tracking level is still needed to confirm final contouring qualities when these approaches are utilized.

Some contouring control architectures, which involve coordinate transformation techniques, such as tangent-normal (*T-N*) coordinate frame (Ho et al., 1998; Chiu & Tomizuka, 2001; Wang & Zhang, 2004; Hsieh et al., 2006) and polar coordinate frame (Chen et al., 2002) have been presented in recent years. For *T-N* coordinate transformation approaches, contouring dynamics are decomposed into tangential and normal directions, where the tangential dynamics is associated with feed-rates while the normal dynamics is relevant to contouring error. Nevertheless, only the contour error of straight paths can be evaluated exactly. The normal errors just stand for approximated contour errors for arbitrary non-linear curves. On the other hand for polar coordinate transformation scheme, dynamics of radial orientation is derived in consideration of both circular and noncircular profiles. The polar coordinate based contouring control framework is adequate for circular profiles. For non-circular profiles, the precision of contouring error estimation relies upon that the radius variation with respect to angle change is small. However, for a given straight line which is (almost) perpendicular to x-axis may not satisfy this assumption.

For the preceding coordinate transformation based contouring control schemes, the main advantage is that the goal of contouring controller design becomes clear and simple; in other words, a tangential controller focuses on maintaining a desired feed-rate while a normal/radial controller is applied to eliminate normal/radial errors. However, good contouring performance still depends on good tracking results when applying the *T-N* coordinate transformation methods. Once a large tracking error occurs, the contouring quality will be degraded considerably.

In order to complete contouring tasks efficiently and accurately, an adequate control strategy is prerequisite. Computed torque method, which uses the nominal dynamic model of the robots to decouple and to linearize the nonlinear system, is one of the well-known

approaches. However, when utilizing the computed torque method only, the resultant performance may not be satisfactory due to the effects caused by lump perturbations including uncertain parameters, modeling errors, load variations and nonlinear friction effects. For the sake of system robustness enhancement, several robust control theories such as learning control (Sun et al., 2006), H-infinity (Fang & Chen, 2002), sliding mode control (SMC) (Zhu et al., 1992; Chen & Xu, 1999) and adaptive control (Slotine & Li, 1988; Dong & Kuhnert, 2005; Lee et al., 2005) have been proposed. In recent decades, SMC and adaptive algorithm have been widely used to control of robot systems. Known as robust and accurate, SMC is a good candidate when systems are interfered by model uncertainties and exogenous disturbances. On the other hand, adaptive algorithm, which possesses learning behavior, is capable of estimating uncertain parameters when the parameters are not precisely known. Therefore in this study, by considering well known backstepping design technique, an integral type SMC is designed together with an adaptation law such that the controlled robotic system is robust against lumped perturbations and an adequate switching gain used in sliding controller is determined systematically without try and error and tedious analysis.

2. Main Concerned Issues and Contributions on Robot Contouring Control Systems

For concerning control of robot manipulator, the main control objective is to control the motion trajectory of the end-effector following a prescribed contour. For conventional trajectory control, a given profile in work space is decoded into independent reference joint positions and the success in contouring control task depends on tracking capability of individual robot joint. However, as argued in the preceding section, once one of the robot joint does not perform good tracking result, the end-effector may deviate from the desired path seriously. Therefore, the contouring control problem on a multi-link robot manipulator leads to a synchronization task of joint position, which can also be referred to as master-slave control scheme (Sarachik & Ragazzini, 1957). Moreover, it has been illustrated by a couple of experiments that good contouring quality doesn't necessary depend on good tracking performance (Peng & Chen, 2007a). Consequently for manipulator contouring control, how to relax tracking capability and preserve contouring precision becomes the main concerned issue in this chapter.
To fulfill the main object mentioned above, some short-term tasks must be considered:

(i) Define an equivalent contour error.
(ii) Derive a contour error model for robotic system.
(iii) Design robust contouring controllers.

For task (i), it is well known that a closed-form solution of the exact contour error for an arbitrary curve is quite difficult to formulate. Thus, approximated contour error estimations are usually applied. Due to the use of inexact contour error models, attenuation of the approximated contour errors may not guarantee the elimination of real contour error especially in the presence of large tracking errors. As a result, an adequate equivalent error index should be defined. In this work, a new error variable named contour index (CI) is given by means of a geometric way in a virtual contouring space (VCS). The properties include: i) the CI is able to act as an equivalent contouring error and replace the normal

tracking error (Hsieh et al., 2006, Chen & Lin, 2008) to be a new performance index without causing geometric over estimation and ii) the CI contributes to contour following behavior (Peng & Chen, 2007a). This phenomenon can be illustrated by referring Fig. 2, where the end-effector at *A* approaches to the real time command *D* through the desired profile instead of moving along $\overrightarrow{AD}$ directly.

Regarding task (ii), the design processes are summarized as follows: dynamic correlation between joint space and work space is firstly established. The work space dynamics are further derived into the VCS, which consists of tangential and normal dynamics. Then, a dynamic equation of CI, which offers the end-effector to trail the prescribed path, is derived. Finally, based on the developed error dynamics, an adaptive sliding controller together with the idea of inverse dynamics control (Spong & Vidyasagar, 1989) is applied to provide system robustness against lumped uncertainties and fulfill the main control object.

The advantage of the proposed method for manipulator contouring control problem contains:

(1) The derivation of contour error model for robotic system is systematic
(2) The closed-loop stability analysis is clear.
(3) Final contouring quality can be maintained even if the end-effector doesn't track the real time command very well.
(4) The proposed method is also extendable to three-dimensional case (Peng & Chen, 2007b).

3. Proposed Contouring Control Framework for a Robot Manipulator

3.1 Forward kinematics

By using the Euler-Lagrange method, a dynamic equation of a vertical robot arm can be expressed as

$$\mathbf{M}(\boldsymbol{\theta})\ddot{\boldsymbol{\theta}} + \mathbf{C}\left(\boldsymbol{\theta},\dot{\boldsymbol{\theta}}\right)\dot{\boldsymbol{\theta}} + \mathbf{G}(\boldsymbol{\theta}) = \boldsymbol{\tau} - \mathbf{F} \tag{1}$$

where $\boldsymbol{\theta}$, $\dot{\boldsymbol{\theta}}$ and $\ddot{\boldsymbol{\theta}} \in \Re^n$ are the joint position, velocity and acceleration vectors, respectively. $\mathbf{M}(\boldsymbol{\theta}) \in \Re^{n\times n}$ is a positive definite inertia matrix; $\mathbf{C}\left(\boldsymbol{\theta},\dot{\boldsymbol{\theta}}\right) \in \Re^{n\times n}$ is a matrix containing Coriolis and centrifugal terms; $\mathbf{G}(\boldsymbol{\theta}) \in \Re^n$ stands for gravitational term; $\boldsymbol{\tau} \in \Re^n$ represents a torque vector and $\mathbf{F} \in \Re^n$ is a disturbance vector referred to nonlinear friction effects. In this study, a two degree of freedom robot ($n = 2$) is considered and depicted in Fig. 3. The position translation from joint space to work space can be calculated by considering forward kinematics as follows,

$$\mathbf{P}_a = h(\boldsymbol{\theta}(t)) \tag{2}$$

Taking the twice time derivative of (2) gives

$$\ddot{\mathbf{P}}_a = \dot{\mathbf{J}}\dot{\boldsymbol{\theta}} + \mathbf{J}\ddot{\boldsymbol{\theta}} \tag{3}$$

where $\mathbf{P}_a = [x \quad y]^T$ is the end-effector position vector in work space, $\mathbf{J}$ is the Jacobian matrix and T denotes the transpose. Note that the Jacobian matrix is assumed to be fully

known for position measurement and is nonsingular during the whole contouring control processes. The definition of matrices used in (2) and (3) are listed in Appendix.

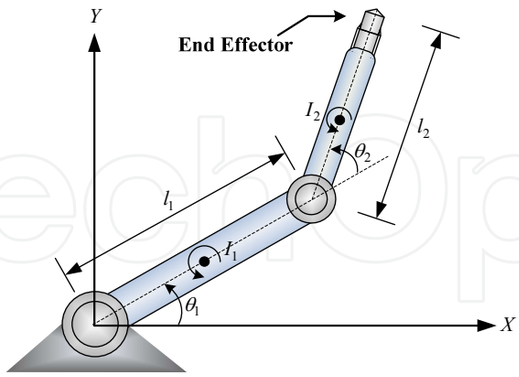

Fig. 3. Two degree of freedom robot.

3.2 Contour generation

Consider a desired profile in work space generated by

$$\mathbf{P_d} = \mathbf{T}_\beta \boldsymbol{\kappa} \overline{\mathbf{P}}_\mathbf{d} + \mathbf{c_o} \tag{4}$$

where $\mathbf{P_d} = [x_d \quad y_d]^T$ and $\overline{\mathbf{P}}_\mathbf{d} = [\overline{x}_d \quad \overline{y}_d]^T$ are position vectors in work space and VCS, respectively. As an example, a standard unit circle in VCS is made up of $\overline{x}_d = \sin(2\pi ft)$ and $\overline{y}_d = \cos(2\pi ft)$, where the frequency f is relative to tangential velocity. $\mathbf{T}_\beta$ denotes a rotational matrix with a angle β and the diagonal gain matrix $\boldsymbol{\kappa}$ (please see Appendix) is relative to the length of major axis and minor axis of the desired profile. The term $\mathbf{c_o} = [c_{xo} \quad c_{yo}]^T$ denotes a shifting operator. The geometric meaning of (4) is depicted in Fig. 4, where an oblique ellipse can be generated from a unit circle by the matrix operation, $\mathbf{T}_\beta \boldsymbol{\kappa}$.

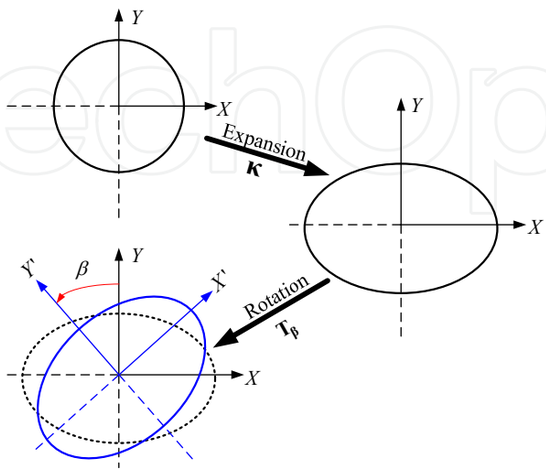

Fig. 4. Command generation via matrix operation.

3.3 Derivation of contour error dynamics

Define the tracking error in work space as $\mathbf{e} = \mathbf{P}_d - \mathbf{P}_a = [e_x \quad e_y]^T$ and then the resulting error dynamics is

$$\ddot{\mathbf{e}} = \ddot{\mathbf{P}}_d - \ddot{\mathbf{P}}_a \tag{5}$$

Subsequently, the error relationship between VCS and work space can be represented by

$$\boldsymbol{\varepsilon} = \mathbf{T}(\mathbf{T}_\beta \boldsymbol{\kappa})^{-1} \mathbf{e} \tag{6}$$

where $\boldsymbol{\varepsilon} = [\varepsilon_n \quad \varepsilon_t]^T$ denotes a transformed error vector including normal tracking error and tangential tracking error. The projection-matrix $\mathbf{T}$ is orthogonal, continuous and differentiable, defined by

$$\mathbf{T} = \begin{bmatrix} -\sin\gamma & \cos\gamma \\ \cos\gamma & \sin\gamma \end{bmatrix} \tag{7}$$

where γ is an instantaneous inclination of the tangential direction corresponding to the circular profile shown in Fig. 5. From the definition of tracking error in work space, Eq. (6) can be rewritten as

$$\boldsymbol{\varepsilon} = \mathbf{T}\left(\mathbf{T}_\beta \boldsymbol{\kappa}\right)^{-1}\left(\mathbf{P}_d - \mathbf{P}_a\right) = \mathbf{T}\underbrace{\left[\overline{\mathbf{P}}_d - \overline{\mathbf{P}}_a\right]}_{\mathbf{E}} + \mathbf{T}\left(\mathbf{T}_\beta \boldsymbol{\kappa}\right)^{-1}\mathbf{c}_o \tag{8}$$

where $\overline{\mathbf{P}}_a = (\mathbf{T}_\beta \boldsymbol{\kappa})^{-1}\mathbf{P}_a$ and $\mathbf{E} = [E_x \quad E_y]^T$. The corresponding geometrical meaning is shown in Fig. 5. Eq. (8) means that the information in the work space is transformed into the VCS through $\mathbf{T}(\mathbf{T}_\beta \boldsymbol{\kappa})^{-1}$; namely, the vectors $\mathbf{P}_a$, $\mathbf{P}_d$ and $\|\mathbf{e}\|$ in the work space are transformed to be $\overline{\mathbf{P}}_a$, $\overline{\mathbf{P}}_d$ and $\|\mathbf{E}\|$ in VCS, respectively. Then the error vector $\|\mathbf{E}\|$ can be further decomposed into tangential and normal directions through the matrix $\mathbf{T}$.

Fig. 5 shows that a moving *T-N* coordinate attaching to the profile guides $\overline{\mathbf{P}}_a$ to follow $\overline{\mathbf{P}}_d$ along the profile. In the control point of view, Eq. (8) also indicates that $\mathbf{P}_d - \mathbf{P}_a = 0$ if and only if $\boldsymbol{\varepsilon} = 0$. Therefore, the control problem turns into a regulation problem in both tangential and normal directions.

From (6)-(7), since $\mathbf{T}^{-1} = \mathbf{T}$, it follows

$$\ddot{\boldsymbol{\varepsilon}} + 2\mathbf{T}\dot{\mathbf{T}}\dot{\boldsymbol{\varepsilon}} + \mathbf{T}\ddot{\mathbf{T}}\boldsymbol{\varepsilon} = \mathbf{T}\left(\mathbf{T}_\beta \boldsymbol{\kappa}\right)^{-1}\ddot{\mathbf{e}} \tag{9}$$

Substituting (5) into (9) yields

$$\begin{aligned} \ddot{\boldsymbol{\varepsilon}} + 2\mathbf{T}\dot{\mathbf{T}}\dot{\boldsymbol{\varepsilon}} + \mathbf{T}\ddot{\mathbf{T}}\boldsymbol{\varepsilon} &= \mathbf{T}\left(\mathbf{T}_\beta \boldsymbol{\kappa}\right)^{-1}\left(\ddot{\mathbf{P}}_d - \ddot{\mathbf{P}}_a\right) \\ &= \mathbf{T}\left(\mathbf{T}_\beta \boldsymbol{\kappa}\right)^{-1}\ddot{\mathbf{P}}_d - \mathbf{T}\left(\mathbf{T}_\beta \boldsymbol{\kappa}\right)^{-1}\left(\dot{\mathbf{J}}\dot{\boldsymbol{\theta}} + \mathbf{J}\ddot{\boldsymbol{\theta}}\right) \\ &= \mathbf{T}\left(\mathbf{T}_\beta \boldsymbol{\kappa}\right)^{-1}\ddot{\mathbf{P}}_d - \mathbf{T}\left(\mathbf{T}_\beta \boldsymbol{\kappa}\right)^{-1}\dot{\mathbf{J}}\dot{\boldsymbol{\theta}} - \mathbf{T}\left(\mathbf{T}_\beta \boldsymbol{\kappa}\right)^{-1}\mathbf{J}\left[\mathbf{M}^{-1}\left(\boldsymbol{\tau} - \mathbf{f} - \mathbf{C}\dot{\boldsymbol{\theta}} - \mathbf{G}\right)\right] \\ &= \boldsymbol{\Sigma} + \mathbf{f}_\varepsilon - \boldsymbol{\Gamma}\boldsymbol{\tau} \end{aligned} \tag{10}$$

where $\boldsymbol{\Sigma} = \mathbf{T}\left(\mathbf{T}_{\beta}\boldsymbol{\kappa}\right)^{-1}\left(\ddot{\mathbf{P}}_{\mathbf{d}} - \dot{\mathbf{J}}\dot{\boldsymbol{\theta}}\right) + \boldsymbol{\Gamma}\left(\mathbf{C}\dot{\boldsymbol{\theta}} + \mathbf{G}\right)$, $\mathbf{f}_{\boldsymbol{\varepsilon}} = \boldsymbol{\Gamma}\mathbf{f}$ and $\boldsymbol{\Gamma} = \mathbf{T}\left(\mathbf{T}_{\beta}\boldsymbol{\kappa}\right)^{-1}\mathbf{J}\mathbf{M}^{-1}$. Eq. (10) represents the error dynamics in the VCS.

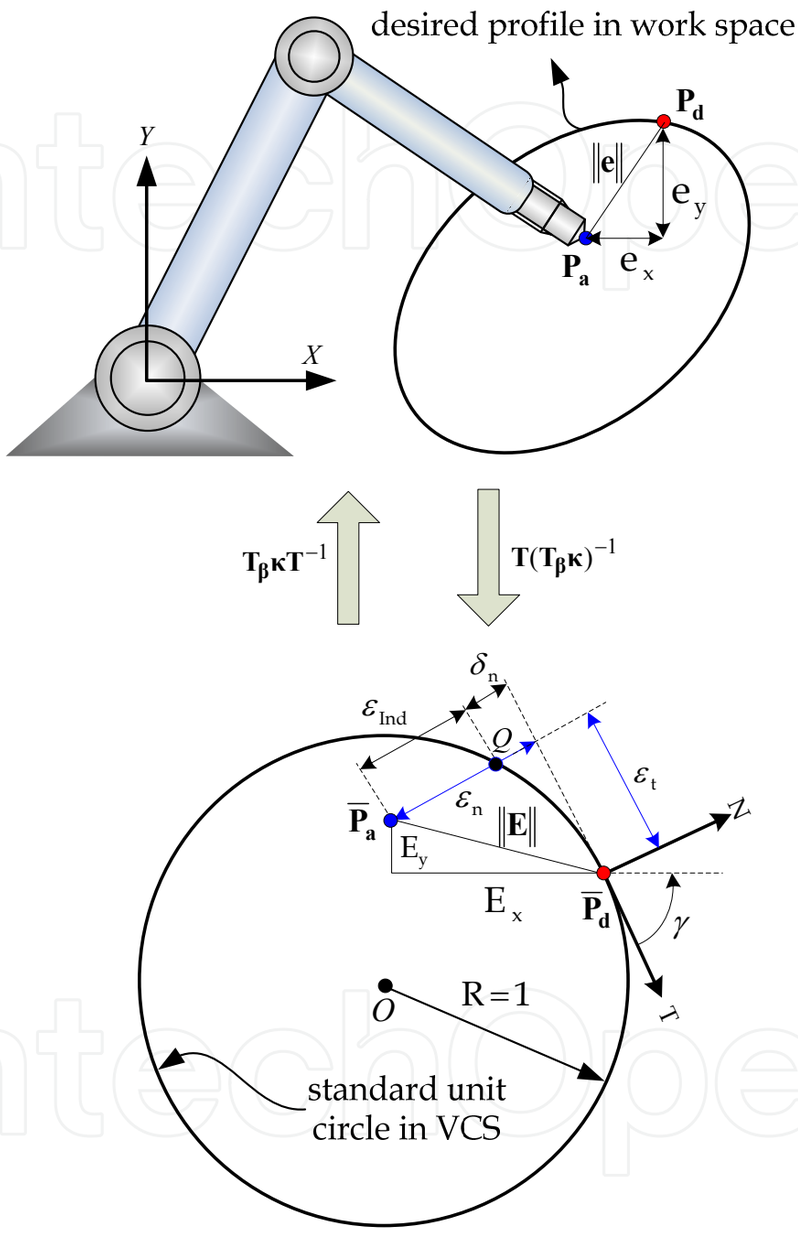

Fig. 5. Robot contouring system.

Consider the inverse dynamics compensation method (Spong & Vidyasagar, 1989), a nominal control torque $\boldsymbol{\tau} = [\tau_1 \quad \tau_2]^{\mathrm{T}}$ for (10) is chosen as the form

$$\boldsymbol{\tau} = \hat{\boldsymbol{\Gamma}}^{-1}\left(\hat{\boldsymbol{\Sigma}} - \boldsymbol{\tau}_{\boldsymbol{\varepsilon}}\right) \tag{11}$$

where $\hat{\mathbf{\Gamma}}$ and $\hat{\mathbf{\Sigma}}$ are denoted as the nominal value of $\mathbf{\Gamma}$ and $\mathbf{\Sigma}$ (i.e., $\mathbf{\Gamma}=\hat{\mathbf{\Gamma}}+\tilde{\mathbf{\Gamma}}$, $\mathbf{\Sigma}=\hat{\mathbf{\Sigma}}+\tilde{\mathbf{\Sigma}}$), respectively and $\boldsymbol{\tau}_{\varepsilon}=[\tau_{\varepsilon n} \quad \tau_{\varepsilon t}]^{\mathrm{T}}$.
Substituting (11) into (10) yields

$$\begin{aligned}\ddot{\boldsymbol{\varepsilon}}+2\mathbf{T}\dot{\mathbf{T}}\dot{\boldsymbol{\varepsilon}}+\mathbf{T}\ddot{\mathbf{T}}\boldsymbol{\varepsilon}&=\mathbf{\Sigma}+\mathbf{f}_{\varepsilon}-\mathbf{\Gamma}\boldsymbol{\tau}\\&=\mathbf{\Sigma}+\mathbf{f}_{\varepsilon}-\hat{\mathbf{\Gamma}}\left[\hat{\mathbf{\Gamma}}^{-1}\left(\hat{\mathbf{\Sigma}}-\boldsymbol{\tau}_{\varepsilon}\right)\right]-\tilde{\mathbf{\Gamma}}\boldsymbol{\tau}\\&=\tilde{\mathbf{\Sigma}}-\tilde{\mathbf{\Gamma}}\boldsymbol{\tau}+\mathbf{f}_{\varepsilon}+\boldsymbol{\tau}_{\varepsilon}\\&=\mathbf{\Lambda}+\boldsymbol{\tau}_{\varepsilon}\end{aligned} \tag{12}$$

where $\mathbf{\Lambda}=\tilde{\mathbf{\Sigma}}-\tilde{\mathbf{\Gamma}}\boldsymbol{\tau}+\mathbf{f}_{\varepsilon}=[\mathbf{\Lambda}_{\mathrm{n}} \quad \mathbf{\Lambda}_{\mathrm{t}}]^{\mathrm{T}}$ represents model uncertainty and external disturbance (for example, the friction effects). Refer to (9), it can be rewritten as

$$\begin{bmatrix}\ddot{\varepsilon}_{\mathrm{n}}\\ \ddot{\varepsilon}_{\mathrm{t}}\end{bmatrix}+2\begin{bmatrix}0 & \dot{\gamma}\\ -\dot{\gamma} & 0\end{bmatrix}\begin{bmatrix}\dot{\varepsilon}_{\mathrm{n}}\\ \dot{\varepsilon}_{\mathrm{t}}\end{bmatrix}-\begin{bmatrix}\dot{\gamma}^{2} & -\ddot{\gamma}\\ \ddot{\gamma} & \dot{\gamma}^{2}\end{bmatrix}\begin{bmatrix}\varepsilon_{\mathrm{n}}\\ \varepsilon_{\mathrm{t}}\end{bmatrix}=\begin{bmatrix}\mathbf{\Lambda}_{\mathrm{n}}+\tau_{\varepsilon n}\\ \mathbf{\Lambda}_{\mathrm{t}}+\tau_{\varepsilon t}\end{bmatrix} \tag{13}$$

Providing the desired feed-rate is set to be constant for predetermined profiles, it follows $\ddot{\gamma}=0$.
From Fig. 5, one can find that the mismatched term δ_{n} in normal direction is caused by the existence of ε_{t} . Thus, the elimination of normal tracking error ε_{n} causes an over-cutting segment δ_{n} when $\varepsilon_{\mathrm{t}}\neq 0$. In order to solve this problem, the CI is introduced in the VCS and is defined by

$$\varepsilon_{\mathrm{Ind}}=\varepsilon_{\mathrm{n}}-\delta_{\mathrm{n}} \tag{14}$$

where $\delta_{\mathrm{n}}=\mathrm{R}-(\mathrm{R}^{2}-\varepsilon_{\mathrm{t}}^{2})^{1/2}$. Note that the CI replaces ε_{n} to be a new performance index or to be regarded as an equivalent contouring error during control process; to put it simply, the purpose of the contouring control is to eliminate $\varepsilon_{\mathrm{Ind}}$ instead of ε_{n} while $\varepsilon_{\mathrm{t}}\neq 0$. Invoking (13) with (14) yields

$$\ddot{\varepsilon}_{\mathrm{Ind}}=\tau_{\varepsilon n}+\eta_{1}+\eta_{2}+\eta_{3}+\mathbf{\Lambda}_{\mathrm{n}} \tag{15}$$

where

$$\begin{cases}\eta_{1}=-2\dot{\gamma}\dot{\varepsilon}_{\mathrm{t}}+\dot{\gamma}^{2}\varepsilon_{\mathrm{n}}-\ddot{\gamma}\varepsilon_{\mathrm{t}}-\left(\varepsilon_{\mathrm{t}}\dot{\varepsilon}_{\mathrm{t}}\right)^{2}\cdot\sigma^{-3/2}-\left[\dot{\varepsilon}_{\mathrm{t}}^{2}+\varepsilon_{\mathrm{t}}\left(2\dot{\gamma}\dot{\varepsilon}_{\mathrm{n}}+\ddot{\gamma}\varepsilon_{\mathrm{n}}+\dot{\gamma}^{2}\varepsilon_{\mathrm{t}}\right)\right]\cdot\sigma^{-1/2}\\ \eta_{2}=-\varepsilon_{\mathrm{t}}\mathrm{u}_{\mathrm{t}}\sigma^{-1/2}\\ \eta_{3}=-\varepsilon_{\mathrm{t}}\mathbf{\Lambda}_{\mathrm{t}}\sigma^{-1/2}\\ \sigma=\mathrm{R}^{2}-\varepsilon_{\mathrm{t}}^{2}\end{cases}$$

Examining (14) again, it is necessary to remind that for all the control period, the condition $|\varepsilon_{\mathrm{t}}|<\mathrm{R}$ must be guaranteed. Consequently, the maximum allowable tracking error in tangential direction is R , which is not a crucial condition in practice.

Therefore, the modified system dynamics in VCS becomes

$$\ddot{\varepsilon}_{\mathrm{t}} - 2\dot{\gamma}\dot{\varepsilon}_{\mathrm{n}} - \dot{\gamma}^2\varepsilon_{\mathrm{t}} = \mathbf{\Lambda}_{\mathrm{t}} + \tau_{\varepsilon t} \tag{16.a}$$

$$\ddot{\varepsilon}_{\mathrm{Ind}} = \eta_1 + \eta_2 + \eta_3 + \mathbf{\Lambda}_{\mathrm{n}} + \tau_{\varepsilon n} \tag{16.b}$$

For (16), contouring controller design will be addressed in the next section.

4. Contouring Controller Design

In this section, design of contouring controller is considered separately for tangential and modified normal dynamics. For demonstration purpose, a general proportional-derivative (PD) controller is applied in tangential error equation. It is well known that the PD controller is capable of achieving stabilization and improving transient response, but is not adequate for error elimination. Consequently, tangential tracking errors exist unavoidably. Under this circumstance, we are going to show that precise contouring performance can still be achieved by applying the CI approach. Building on the developed contouring control framework, the tangential and normal control objects can be respectively interpreted as stabilization and regulation problems.

4.1 Design of tangential control effort

Considering the tangential dynamics of (16.a), a PD controller with the form

$$\tau_{\varepsilon t} = -\mathrm{K}_{\mathrm{Vt}}\dot{\varepsilon}_{\mathrm{t}} - \mathrm{K}_{\mathrm{Pt}}\varepsilon_{\mathrm{t}} - 2\dot{\gamma}\dot{\varepsilon}_{\mathrm{n}} - \dot{\gamma}^2\varepsilon_{\mathrm{t}} \tag{17}$$

is applied. Substituting (17) into (16.a) results in

$$\ddot{\varepsilon}_{\mathrm{t}} + \mathrm{K}_{\mathrm{Vt}}\dot{\varepsilon}_{\mathrm{t}} + \mathrm{K}_{\mathrm{Pt}}\varepsilon_{\mathrm{t}} = \mathbf{\Lambda}_{\mathrm{t}} \tag{18}$$

where K_{Vt} and K_{Pt} are positive real. The selection of control gains should guarantee the criterion $|\varepsilon_{\mathrm{t}}| < \mathrm{R}$. Eq. (18) indicates that the tangential tracking error cannot be eliminated very well due to the existence of $\mathbf{\Lambda}_{\mathrm{t}}$. However, it will be shown that the existence of ε_{t} causes no harm to contouring performance with the aid of CI.

4.2 Design of normal control effort

In the following, an integral type sliding controller for the modified normal dynamics is developed by using backstepping approach. Firstly, let $\varepsilon_{\mathrm{Ind}} = \varepsilon_{\mathrm{Ind1}}$ and define an internal state w. Then the system (16.b) can be represented as

$$\dot{\mathrm{w}} = \varepsilon_{\mathrm{Ind1}} \tag{19.a}$$

$$\dot{\varepsilon}_{\mathrm{Ind1}} = \varepsilon_{\mathrm{Ind2}} \tag{19.b}$$

$$\dot{\varepsilon}_{\mathrm{Ind2}} = \eta_1 + \eta_2 + \eta_3 + \mathbf{\Lambda}_{\mathrm{n}} + \tau_{\varepsilon n} \tag{19.c}$$

Assume that the system state $\varepsilon_{\text{Ind1}}$ can be treated as an independent input $\phi_1(\text{w})$, and let

$$\varepsilon_{\text{Ind1}} = \phi_1 = -\text{k}_1\text{w} \tag{20}$$

where $\text{k}_1 > 0$. Then, consider as a Lyapunov function

$$\text{V}_1 = \text{w}^2/2 \tag{21}$$

The derivative of (21) is

$$\dot{\text{V}}_1 = \text{w}\phi_1 = -\text{k}_1\text{w}^2 \le 0 \tag{22}$$

In practice, there may exist a difference between $\varepsilon_{\text{Ind1}}$ and ϕ_1. Hence, define a new error variable by $\text{z}_1 = \varepsilon_{\text{Ind1}} - \phi_1$, which gives

$$\dot{\text{w}} = \text{z}_1 + \phi_1 \tag{23.a}$$

and

$$\dot{\text{z}}_1 = \varepsilon_{\text{Ind2}} - \dot{\phi}_1 \tag{23.b}$$

Second, in a similar manner, consider $\varepsilon_{\text{Ind2}}$ as a virtual control input and let

$$\varepsilon_{\text{Ind2}} = \phi_2 = -\text{w} - \text{k}_2\text{z}_1 + \dot{\phi}_1 \tag{24}$$

Selecting as a Lyapunov candidate

$$\text{V}_2 = \text{w}^2/2 + \text{z}_1^2/2 \tag{25}$$

and taking its time derivative gives

$$\begin{aligned} \dot{\text{V}}_2 &= \text{w}(\text{z}_1 + \phi_1) + \text{z}_1(\varepsilon_{\text{Ind2}} - \dot{\phi}_1) \\ &= \text{w}(\text{z}_1 + \phi_1) + \text{z}_1(\phi_2 - \dot{\phi}_1) \\ &= -\text{k}_1\text{w}^2 - \text{k}_2\text{z}_1^2 \le 0 \end{aligned} \tag{26}$$

Note that the criterion (26) is achieved only when the virtual control law (24) comes into effect. Taking the constraint into account, one can design a sliding surface as $\text{z}_2 = \varepsilon_{\text{Ind2}} - \phi_2$, and then the augmented system can be represented as

$$\dot{\text{w}} = \text{z}_1 + \phi_1 \tag{27.a}$$

$$\dot{z}_1 = z_2 + \phi_2 - \dot{\phi}_1 \tag{27.b}$$

$$\dot{z}_2 = \eta_1 + \eta_2 + \eta_3 + \mathbf{\Lambda}_n + \tau_{sn} - \dot{\phi}_2 \tag{27.c}$$

Suppose that the parameter uncertainties and external disturbances satisfy the inequality $\max\left(\left|\eta_3 + \mathbf{\Lambda}_n\right|\right) < \Omega$, where Ω is an unknown positive constant, then the final control object is to develop a controller that provides system robustness against Ω.
Design a control law in the following form

$$\tau_{sn} = -\eta_1 - \eta_2 - z_1 - k_3 z_2 + \dot{\phi}_2 - \xi\,\mathrm{sgn}(z_2) \tag{28}$$

where $\xi \geq \Omega$ denotes the switching gain. Select a Lyapunov candidate as

$$V_3 = w^2/2 + z_1^2/2 + z_2^2/2 \tag{29}$$

From (28) and (29), one can obtain

$$\begin{aligned} \dot{V}_3 &\leq w(z_1 + \phi_1) + z_1\left(z_2 + \phi_2 - \dot{\phi}_1\right) + z_2\left(\eta_1 + \eta_2 - \dot{\phi}_2 + \tau_{sn}\right) + \Omega|z_2| \\ &\leq -k_1 w^2 - k_2 z_1^2 - k_3 z_2^2 - z_2 \xi\,\mathrm{sgn}(z_2) + \Omega|z_2| \\ &= -2kV_3 - |z_2|(\xi - \Omega) \leq -2kV_3 \end{aligned} \tag{30}$$

where $k_1 = k_2 = k_3 = k$ is applied. Therefore, system (27) is exponentially stable by using the control law (28) when the selected ξ satisfies $\xi > \Omega$. Since the upper bound of Ω may not be efficiently determined, the following well known adaptation law (Yoo & Chung, 1992), which dedicates to estimate an adequate constant value ξ_a, is applied

$$\dot{\hat{\xi}}_a = \Psi z_2 \mathrm{sat}(z_2, \rho) \tag{31}$$

where $\hat{\xi}_a$ is denoted as an estimated switching gain and

$$\begin{cases} \Psi > 0 & |z_2| > \rho \\ \Psi = 0 \text{ , } & |z_2| \leq \rho \end{cases} \tag{32}$$

stands for an adaptation gain, where the use of dead-zone is needed due to the face that the ideal sliding does not occur in practical applications. For chattering avoidance, the discontinuous controller (28) is replaced by

$$\tau_{sn} = -\eta_1 - \eta_2 - z_1 - k_3 z_2 + \dot{\phi}_2 - \hat{\xi}_a \mathrm{sat}(z_2, \rho) \tag{33}$$

The saturation function is described as follows

$$\mathrm{sat}(z_2,\rho):=\begin{cases}\mathrm{sgn}(z_2) & |z_2|>\rho\\ z_2/\rho & |z_2|\le\rho\end{cases} \tag{34}$$

where ρ is relative to the thickness of the boundary layer.

Let the estimative error be $\tilde{\xi}_a$, i.e., $\tilde{\xi}_a=\xi_a-\hat{\xi}_a$ and then select a Lyapunov function as

$$V_4=w^2/2+z_1^2/2+z_2^2/2+\tilde{\xi}_a^{\,2}/2\Psi \tag{35}$$

The time derivative of (35) is

$$\begin{aligned}\dot{V}_4&=w\dot{w}+z_1\dot{z}_1+z_2\dot{z}_2+\tilde{\xi}_a\dot{\tilde{\xi}}_a/\Psi\\&\le -k_1w^2-k_2z_1^2-k_3z_2^2-\left(z_2\hat{\xi}_a\mathrm{sat}(z_2,\rho)-\Omega|z_2|\right)-\tilde{\xi}_a z_2\mathrm{sat}(z_2,\rho)\\&=-2kV_4-\left(z_2\xi_a\mathrm{sat}(z_2,\rho)-\Omega|z_2|\right)\\&=-2kV_4-|z_2|\left(\xi_a|z_2|/\rho-\Omega\right)\\&=-2kV_4+\vartheta(t)\end{aligned} \tag{36}$$

where $\vartheta(t)$ is bounded by $|\vartheta(t)|\le\vartheta_{\max}$. In general, $\xi_a\ge\Omega$ is available. Suppose that $\xi_a=\Omega$, it follows $\vartheta(t)=-\Omega|z_2|\left(|z_2|/\rho-1\right)$. The maximum value $\vartheta_{\max}=\rho\Omega/4$ occurs at $|z_2|=\rho/2$. Eq. (36) reveals that for $t\to\infty$, it follows

$$\begin{aligned}V_4(t)&\le\exp(-2kt)V_4(0)+\int_0^t\exp(-2k(t-\upsilon))\vartheta(\upsilon)d\upsilon\\&\le\exp(-2kt)V_4(0)+\frac{\vartheta_{\max}}{2k}\left[1-\exp(-2kt)\right]\le\frac{\rho\Omega}{8k}\end{aligned} \tag{37}$$

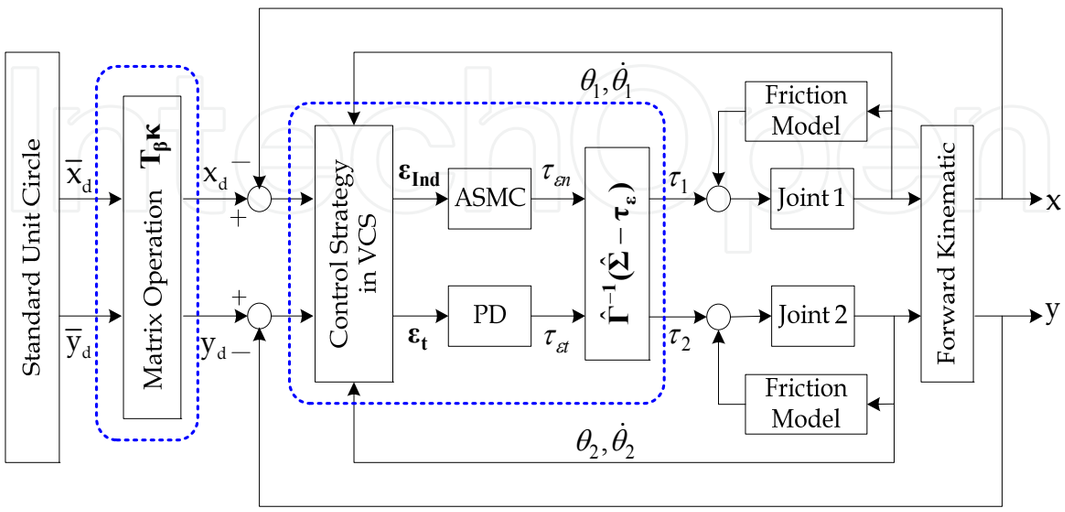

Fig. 6. Block diagram of the proposed contouring control scheme for a 2-Link robotic system.

By (37), the system is exponentially stable with a guaranteed performance associated with the size of control parameters ρ and k . The overall contouring control architecture is illustrated in Fig. 6. It is similar with the standard feedback control loop, where the main control components are highlighted in the dotted blocks.

Remark. 1 For illustration purpose, a PD controller is applied to the tangential dynamics such that tangential tracking error cannot be eliminated completely. Of course one can also apply a robust controller to pursue its performance if necessary. However, the following simulations are going to show that even in the presence of tracking errors, the contouring performance will not be degraded by using the proposed contouring control framework.

Remark. 2 The action of the adaptive law activates when $|z_2| > \rho$. It means that for a given small gain value, $\hat{\xi}_a$ will be renewed in real time until the criterion $|z_2| \le \rho$ is achieved.

5. Numerical Simulations

In this section, a robot system in consideration of nonlinear friction effects is taken as an example. The friction model used in numerical simulations is given by

$$F_i = \mathrm{sgn}(\dot{\theta}_i)\left[F_{ci} + (F_{si} - F_{ci})\exp\left(-(\dot{\theta}_i / \dot{\theta}_{si})^2\right)\right] + \sigma_{si}\dot{\theta}_i \tag{38}$$

where F_{ci} is the Coulomb friction and F_{si} is the static friction force. $\dot{\theta}_{si}$ denotes an angular velocity relative to the Stribeck effect and σ_{si} denotes the viscous coefficient. The suffix $i = 1,2$ indicates the number of robot joint.

The parameters used in friction model are:

$$F_{c1} = 0.025\ ,\ F_{c2} = 0.02\ ,\ F_{s1} = 0.04\ ,\ F_{s2} = 0.035$$
$$\dot{\theta}_{s1} = \dot{\theta}_{s2} = 0.001,\ \sigma_{s1} = 0.005 \text{ and } \sigma_{s2} = 0.004\ .$$

According to the foregoing analysis, an adequate switching gain is suggested to be determined in advance for confirming system robustness. Thus, estimations are performed previously for two contouring control tasks, i.e., circular and elliptical contours. Fig. 7(a) and (c) show the responses of sliding surface and Fig. 7(b) and (d) depict the response of $\hat{\xi}_a$ during update.

From Fig. 7, it implies that the sliding surfaces were suppressed to the prescribed boundary layer by integrating with the adaptation law. The initial guess-value $\hat{\xi}_a(0) = 12$ and the adaptation gain $\Psi = 100$ are applied in (31). According to (32), an adequate value of $\hat{\xi}_a$ was determined when $|z_2| \le \rho = 0.0025$ is achieved. From the adaptation results shown in Fig. 7(b) and 7(d), the conservative switching gains $\hat{\xi}_a = 18$ and 16.5 are adopted to handle circular and elliptical profiles, respectively.

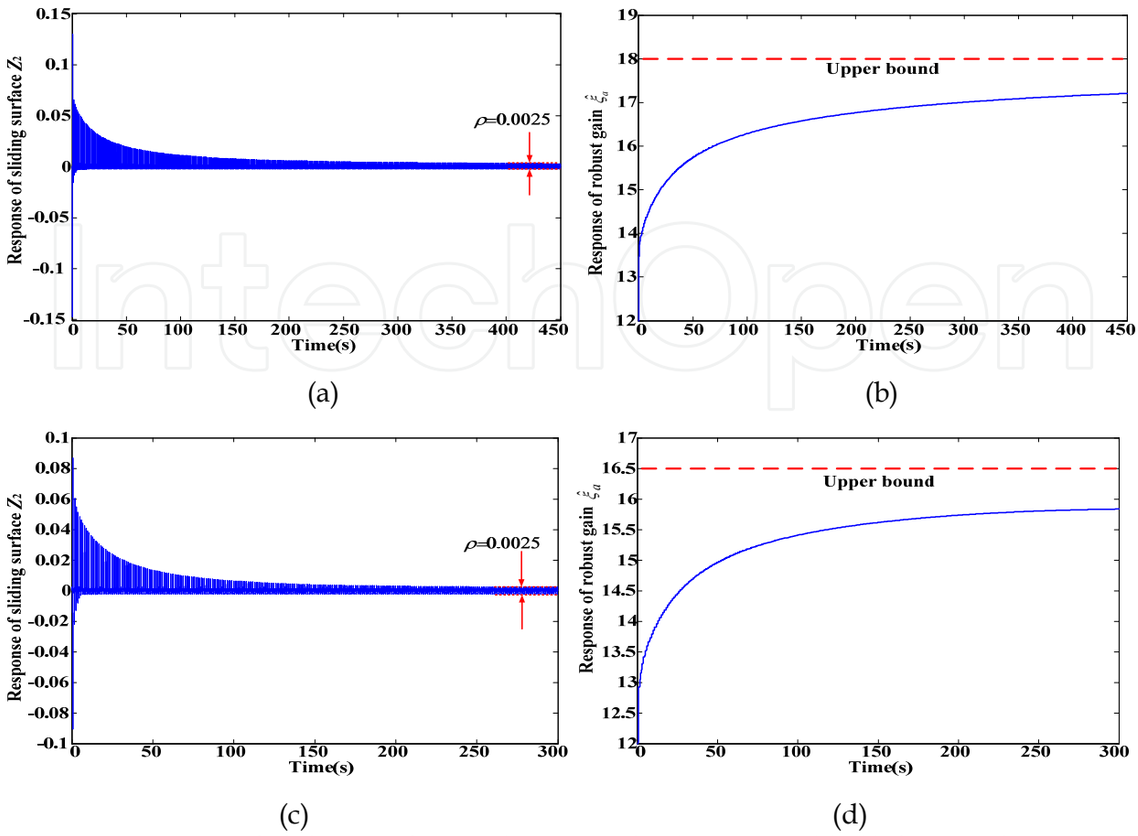

Fig. 7. Responses of sliding surface and estimated robust gain. (a)-(b) for circular contour, (c)-(d) for elliptical contour.

5.1 Circular contour

The following values are used for the control of circular profile:

$$\beta = 0\,,\ \kappa_x = \kappa_y = 0.1\,,\ f = 1\,,\ (c_{xo}\,, c_{yo}) = (0.21\,, 0.15)$$
$$k = 10\,,\ K_{Vt} = 9\,,\ K_{Pt} = 20\,,\ \hat{m}_1 = 7.8\,,\ \hat{m}_2 = 0.37$$

Exact system parameters of two-arm robot are

$$m_1 = 8.344\,,\ m_2 = 0.348\,,\ l_1 = 0.25\,,\ l_2 = 0.21$$

In this case, the position of starting point in the working space is set to be at $\mathbf{P_a}(0) = [x_0 \quad y_0]^T = [0.21 \quad 0.25]^T$. For a given position $\mathbf{P_a}(0)$, initial joint positions can be calculated by applying the inverse kinematics as follows

$$\theta_2(0) = \pm\cos^{-1}\left(\frac{x_0^2 + y_0^2 - l_1^2 - l_2^2}{2l_1 l_2}\right)$$
$$\theta_1(0) = \tan^{-1}\left(\frac{y_0}{x_0}\right) - \tan^{-1}\left(\frac{l_2 \sin\theta_2}{l_1 + l_2\cos\theta_2}\right) \quad (39)$$

Referring to the simulations, Fig. 8 obviously illustrates the contour following behavior. It shows that even though the real time command position (i.e., the moving ring) goes ahead the end-effector, the end-effector still follows to the desired contour without significant deviation. The tracking responses are shown in Fig. 9(a) and (b), where the tracking errors exist significantly, but the contouring performance, evaluated by the contour index ε_{Ind}, remains in a good level. The corresponding control efforts of each robot joint are drawn in Fig.10(a)-(b). Examining Fig. 8(a) and (b) again, it can be seen that the time instants where the relative large tracking errors occur are also the time instants the relative large CIs are induced. The reason can refer to the dynamics of CI given in (16). Due to the face that (16b) is perturbed by the coupling uncertain terms η_3 when $\varepsilon_t \neq 0$, the control performance will be (relatively) degraded when large tangential tracking errors occur.

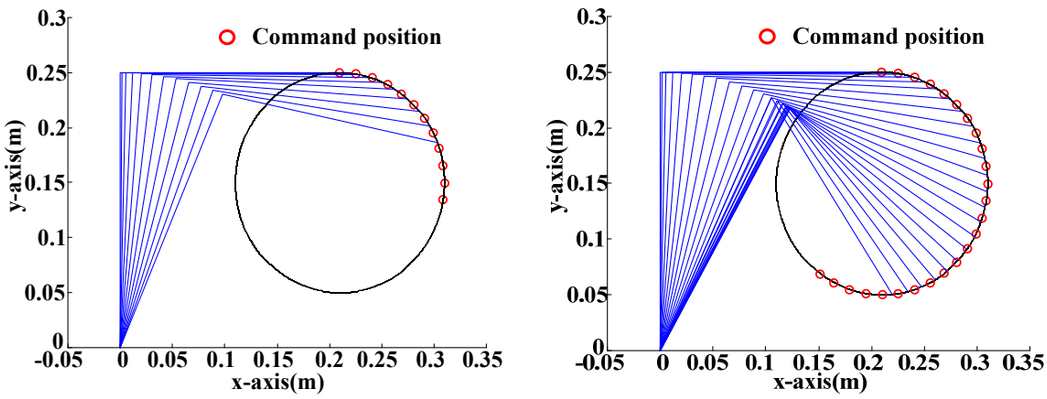

(a) (b)

Fig. 8. Behavior of path following by the proposed method.

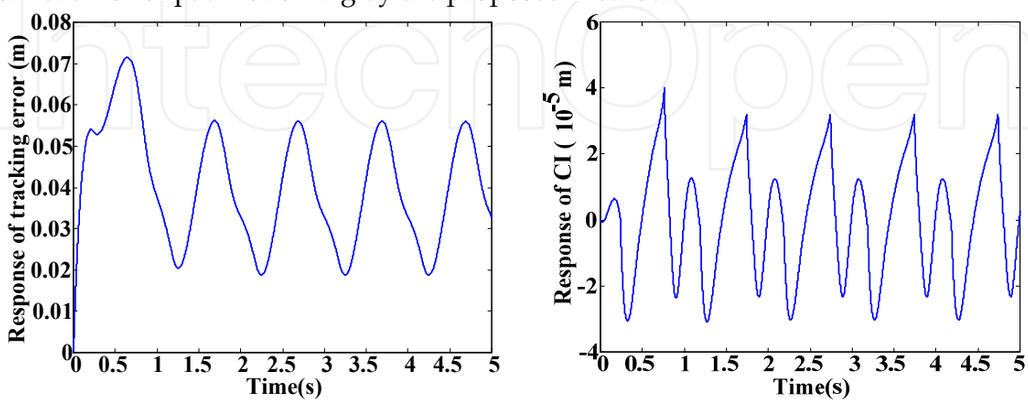

(a) (b)

Fig. 9. Performance of tracking and equivalent contouring errors.

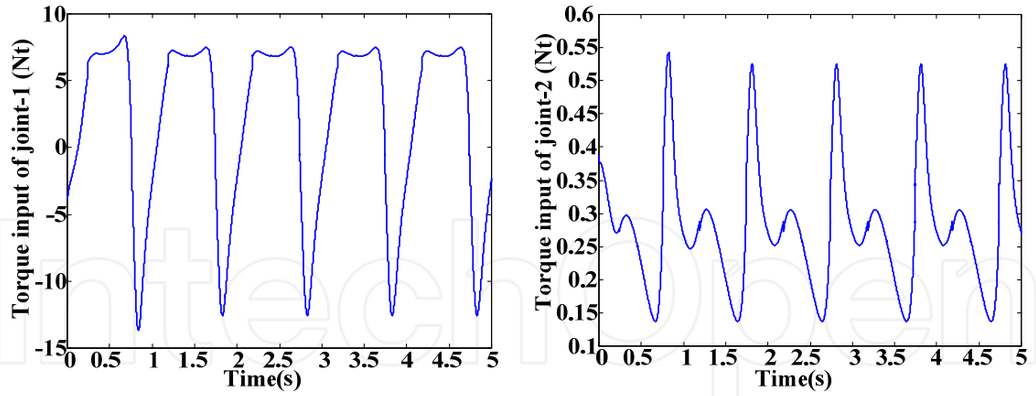

(a) (b)

Fig. 10. Applied control torque.

5.2 Elliptical contour

In this case, the value of parameters are the same with those used in the previous case except $\beta = \pi/3$, $\kappa_x = 0.15$ and $\kappa_y = 0.1$.

Fig. 11 evidently demonstrates that the proposed method confines the motion of the end-effector to the desired contour. The tracking performance and contouring performance are shown in Fig. 12(a) and (b), respectively. The manipulator motion remains attaching on the elliptical profile even though the end-effector doesn't track the real time command precisely. The result is consistent with the behavior illustrated in Fig. 2, i.e., the end-effector at *A* approaches to the real time command *D* through the desired path without causing short cutting phenomenon. Moreover, it has been demonstrated that the CI approach is also capable of avoiding over-cutting phenomenon, which is induced by the *T-N* coordinate transformation approach, in the presence of large tracking errors (Peng & Chen, 2007a). The simulation results confirm again that good contouring control performance does not necessarily rely on the good tracking level. The corresponding continuous control efforts of joint-1 and -2 are shown in Fig. 12(a) and (b), respectively.

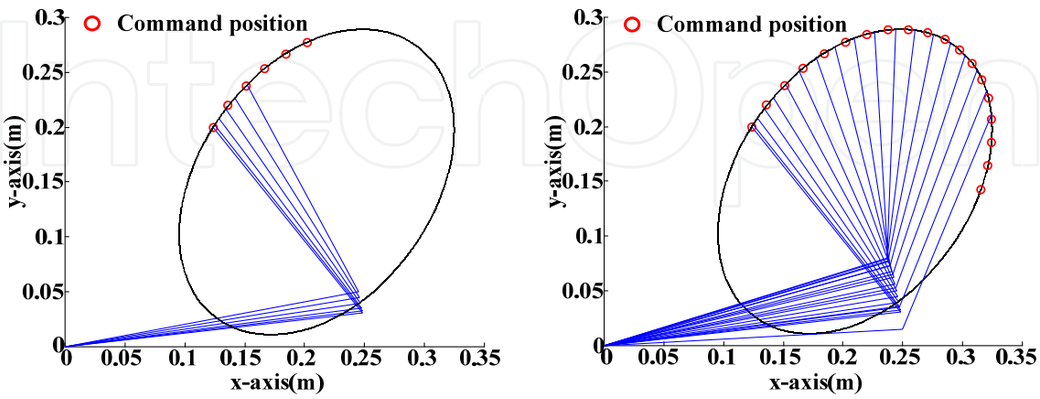

(a) (b)

Fig. 11. Partial behavior of path following by the proposed method.

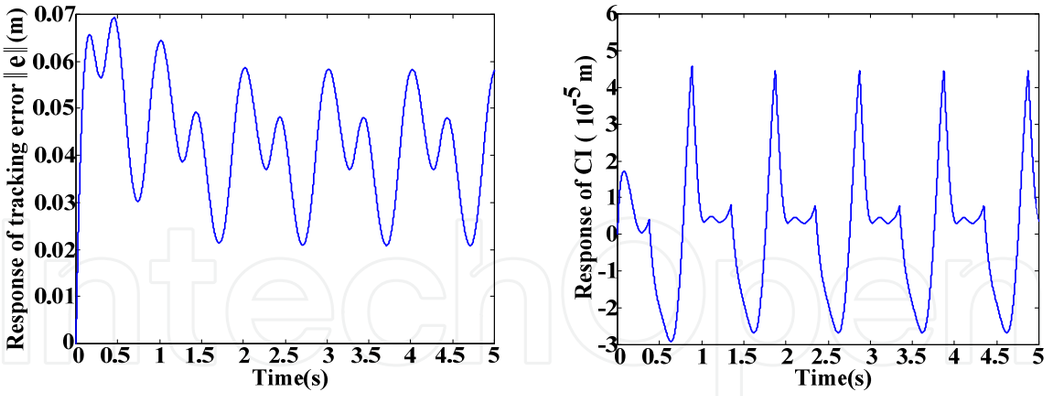

(a) (b)

Fig. 12. Performance of tracking and contouring.

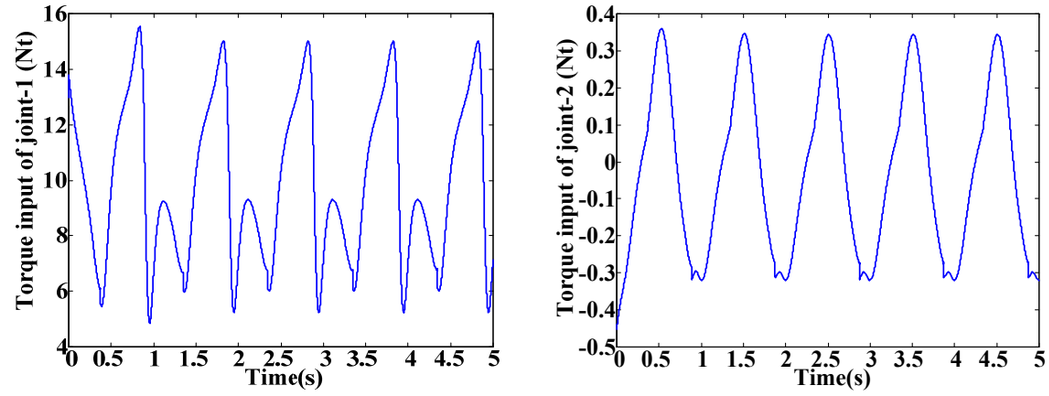

(a) (b)

Fig. 13. Applied control torque.

6. Conclusion

In the robotic motion control field, positioning and tracking are considered as the main control tasks. In this Chapter, we have addressed a specific motion control topic, termed as contouring control. The core concept of the contouring control is different from the main object of the tracking control according to its goal.

For tracking control, the desired goal is to track the real time reference command as precise as possible. On the other hand, the main object is to achieve precise motion along prescribed contours for contouring control. Under this circumstance, tracking error is no longer a necessary performance index requiring to be minimized. To enhance resulting contour precision without relying on tracking performance, a contour following control strategy for robot manipulators is presented.

Different from the conventional manipulator motion control, a contour error dynamics is derived via coordinate transformation and an equivalent error called CI is introduced in VCS to evaluate contouring control performance. The contouring control task in the VCS turns into a stabilizing problem in tangential dynamics and a regulation problem in

modified normal dynamics. The main advantage of the control scheme is that the final contouring accuracy will not be degraded even if the tracking performance of the robot manipulator is not good enough; that is, the existence of tracking errors will not make harm to the final contouring quality. This advantage has been apparently clarified through numerical study.

7. References

Chen, C. L. & Lin, K. C. (2008). Observer-Based Contouring Controller Design of a Biaxial State System Subject to Friction, *IEEE Transactions on Control Systems Technology*, Vol. 16, No. 2, 322-329.

Chen, C. L. & Xu, R. L. (1999). Tracking control of robot manipulator using sliding mode controller with performance robustness, *Journal of Dynamic Systems Measurement and Control-Transactions of the ASME*, Vol. 121, No. 1, 64-70.

Chen, S. L.; Liu, H. L. & Ting, S. C. (2002). Contouring control of biaxial systems based on polar coordinates, *IEEE-ASME Transactions on Mechatronics*, Vol. 7, No. 3, 329-345.

Chin, J. H. & Lin, T. C. (1997). Cross-coupled precompensation method for the contouring accuracy of computer numerically controlled machine tools, *International Journal of Machine Tools and Manufacture*, Vol. 37, No. 7, 947–967.

Chiu, G.T.-C. & Tomizuka, M. (2001). Contouring control of machine tool feed drive systems: a task coordinate frame approach, *IEEE Transactions on Control Systems Technology*, Vol. 9, No. 1, 130-139.

Dong, W. & Kuhnert, K. D. (2005) Robust adaptive control of nonholonomic mobile robot with parameter and nonparameter uncertainties, *IEEE Transactions on Robotics*, Vol. 21, No. 2, 261-266.

Fang, R. W. & Chen, J. S. (2002). A cross-coupling controller using an H-infinity scheme and its application to a two-axis direct-drive robot, *Journal of Robotic Systems,* Vol. 19, No. 10, 483-497.

Feng, G. & Palaniswami, M. (1993). Adaptive control of robot manipulators in task space, *IEEE Transactions on Automatic Control,* Vol. 38, No. 1, 100-104.

Ho, H. C.; Yen, J. Y. & Lu, S. S. (1998). A decoupled path-following control algorithm based upon the decomposed trajectory error, *International Journal of Machine Tools and Manufacture*, Vol. 39, No. 10, 1619-1630.

Hsieh, C.; Lin, K. C. & Chen, C. L. (2006). Contour Controller Design for Two-dimensional Stage System with Friction, *Material Science Forum,* Vol. 505-507, 1267-1272.

Koren, Y. (1980). Cross-Coupled Biaxial Computer Control for Manufacturing Systems, *Journal of Dynamic Systems Measurement and Control-Transactions of the ASME,* Vol. 102, No. 4, 265-272.

Lee, J. H.; Dixon, W. E.; Ziegert, J. C. & Makkar, C. (2005). Adaptive nonlinear contour coupling control for a machine tool system, *IEEE/ASME International Conference on Advanced Intelligent Mechatronics. Proceedings*, 1629 – 1634.

Peng, C. C. & Chen, C. L. (2007a). Biaxial contouring control with friction dynamics using a contour index approach, *International Journal of Machine Tools & Manufacture*, Vol. 2007, No. 10, 1542-1555.

Peng, C. C. & Chen, C. L. (2007b). A 3-dimensional contour following strategy via coordinate transformation for manufacturing applications, *International Conference on Advanced Manufacture*, Tainan, Taiwan, November, Paper No. B4-95.

Ramesh, R.; Mannan, M. A. & Poo, A. N. (2005). Tracking and contour error control in CNC servo systems, *International Journal of Machine Tools and Manufacture*, Vol. 45, No. 3 301-326.

Sarachik, P. & Ragazzini, J. R. (1957). A Two Dimensional Feedback Control System, *Transactions AIEE*, Vol. 76, 55–61.

Shih, Y. T.; Chen, C. S. & Lee, A. C. (2002). A novel cross-coupling control design for Bi-axis motion, *International Journal of Machine Tools and Manufacture*, Vol. 42, No. 14, 1539-1548.

Slotine, J. J. E. & Li, W. P. (1988). Adaptive manipulator control: a case study, *IEEE Transactions on Automatic Control*, Vol. 33, No. 11, 995-1003.

Spong, M. W. & Vidyasagar, M. (1989). *Robot dynamics and control*, John Wiley & Sons, Inc.

Sun, M.; Ge, S. S. & Mareels, I. M. Y. (2006). Adaptive repetitive learning control of robotic manipulators without the requirement for initial repositioning, *IEEE Transactions on Robotics*, Vol. 22, No. 3, 563-568.

Wang, L. S & Zhang, J. (2004). The research of static de-coupled contour control technique of the ultra-precision machine tool, *Proceedings of the 5th World Congress on Intelligent Control and Automation*, June 15-19, Hangzhou, China.

Yeh, S. S. & Hsu, P. L. (1999) Analysis and design of the integrated controller for precise motion systems, *IEEE Transactions on Control Systems Technology*, Vol. 7, No. 6, 706-717.

Zhong, Q.; Shi, Y.; Mo, J. & Huang, S. (2002). A linear cross-coupled control system for high-speed machining, *The International Journal of Advanced Manufacturing Technology*, Vol. 19, No. 8, 558-563.

Zhu, W. H.; Chen, H. T. & Zhang, Z. J. (1992). A variable structure robot control algorithm with an observer, *IEEE Transactions on Robotics and Automation*, Vol. 8, No. 4, 1992, 486-492.

Yoo, D. S. & Chung, M. J. (1992). A variable structure control with simple adaptation laws for upper bounds on the norm of the uncertainties, *IEEE Transactions on Automatic Control*, Vol. 37, No. 6, 860-865.

Acknowledgements

Acknowledgments: Part of this work was supported by the National Science Council, Taiwan, under the Grant No. NSC96-2221-E006-052.

Appendix

The matrices used in this paper for 2-link rigid robot are listed in the following

$$\mathbf{M}=\begin{bmatrix}\mathbf{M}_{11} & \mathbf{M}_{12}\\ \mathbf{M}_{21} & \mathbf{M}_{22}\end{bmatrix},\quad \mathbf{C}=\begin{bmatrix}-2m_2l_1l_{c2}\dot{\theta}_2\sin(\theta_2) & -m_2l_1l_{c2}\dot{\theta}_2\sin(\theta_2)\\ m_2l_1l_{c2}\dot{\theta}_1\sin(\theta_2) & 0\end{bmatrix},$$

$$\mathbf{G}=\begin{bmatrix}m_1gl_{c1}\cos(\theta_1)+m_2g(l_1\cos(\theta_1)+l_{c2}\cos(\theta_1+\theta_2))\\ m_2gl_{c2}\cos(\theta_1+\theta_2)\end{bmatrix}$$

where

$$\mathbf{M}_{11} = \mathrm{m}_1 \mathrm{l}_{c1}^2 + \mathrm{m}_2 \left(\mathrm{l}_1^2 + \mathrm{l}_{c2}^2 + 2\mathrm{l}_1 \mathrm{l}_{c2} \cos(\theta_2) \right) + \mathrm{I}_1 + \mathrm{I}_2$$
$$\mathbf{M}_{12} = \mathrm{m}_2 \left(\mathrm{l}_1 \mathrm{l}_{c2} \cos(\theta_2) + \mathrm{l}_{c2}^2 \right) + \mathrm{I}_2$$
$$\mathbf{M}_{21} = \mathrm{m}_2 \left(\mathrm{l}_1 \mathrm{l}_{c2} \cos(\theta_2) + \mathrm{l}_{c2}^2 \right) + \mathrm{I}_2$$
$$\mathbf{M}_{22} = \mathrm{m}_2 \mathrm{l}_{c2}^2 + \mathrm{I}_2$$
$$\mathrm{l}_{ci} = \frac{1}{2}\mathrm{l}_i, \ \mathrm{I}_i = \frac{1}{12}\mathrm{m}_i \mathrm{l}_i^2$$

The vector used in (2) is

$$\mathrm{h}(\boldsymbol{\theta}(\mathrm{t})) = \begin{bmatrix} \mathrm{l}_1 \cos(\theta_1) + \mathrm{l}_2 \cos(\theta_1 + \theta_2) \\ \mathrm{l}_1 \sin(\theta_1) + \mathrm{l}_2 \sin(\theta_1 + \theta_2) \end{bmatrix}$$

and the Jacobin matrix is defined as

$$\mathbf{J} = \begin{bmatrix} -\mathrm{l}_1 \sin(\theta_1) - \mathrm{l}_2 \sin(\theta_1 + \theta_2) & -\mathrm{l}_2 \sin(\theta_1 + \theta_2) \\ \mathrm{l}_1 \cos(\theta_1) + \mathrm{l}_2 \cos(\theta_1 + \theta_2) & \mathrm{l}_2 \cos(\theta_1 + \theta_2) \end{bmatrix}$$

Regarding command generation, the operation matrices are

$$\mathbf{T}_\beta = \begin{bmatrix} \cos\beta & -\sin\beta \\ \sin\beta & \cos\beta \end{bmatrix}, \ \boldsymbol{\kappa} = \begin{bmatrix} \kappa_x & 0 \\ 0 & \kappa_y \end{bmatrix}$$

IntechOpen

Advances in Robot Manipulators

Edited by Ernest Hall

ISBN 978-953-307-070-4
Hard cover, 678 pages
Publisher InTech
Published online 01, April, 2010
Published in print edition April, 2010

The purpose of this volume is to encourage and inspire the continual invention of robot manipulators for science and the good of humanity. The concepts of artificial intelligence combined with the engineering and technology of feedback control, have great potential for new, useful and exciting machines. The concept of eclecticism for the design, development, simulation and implementation of a real time controller for an intelligent, vision guided robots is now being explored. The dream of an eclectic perceptual, creative controller that can select its own tasks and perform autonomous operations with reliability and dependability is starting to evolve. We have not yet reached this stage but a careful study of the contents will start one on the exciting journey that could lead to many inventions and successful solutions.

InTech Europe
University Campus STeP Ri
Slavka Krautzeka 83/A
51000 Rijeka, Croatia
Phone: +385 (51) 770 447
Fax: +385 (51) 686 166
www.intechopen.com

InTech China
Unit 405, Office Block, Hotel Equatorial Shanghai
No.65, Yan An Road (West), Shanghai, 200040, China
中国上海市延安西路65号上海国际贵都大饭店办公楼405单元
Phone: +86-21-62489820
Fax: +86-21-62489821

IntechOpen